Magnesium-assisted hydrogen improves isoproterenol-induced heart failure

Fengbao Chen[1,#], Ruimin Chen[1,#], Lili Yang[1,2], Bowen Shen[1,3], Yunting Wang[1], Yongfeng Gao[1], Rui Tan[1,*], Xiaomin Zhao[1,*]

https://doi.org/10.4103/mgr.MEDGASRES-D-24-00135

Date of submission: December 6, 2024

Date of decision: February 7, 2025

Date of acceptance: March 19, 2025

Date of web publication: April 29, 2025

Abstract

Heart failure (HF) is a leading cause of mortality among patients with cardiovascular disease and is often associated with myocardial apoptosis and endoplasmic reticulum stress (ERS). While hydrogen has demonstrated potential in reducing oxidative stress and ERS, recent evidence suggests that magnesium may aid in hydrogen release within the body, further enhancing these protective effects. This study aimed to investigate the cardioprotective effects of magnesium in reducing apoptosis and ERS through hydrogen release in a rat model of isoproterenol (ISO)-induced HF. Magnesium was administered orally to ISO-induced HF rats, which improved cardiac function, reduced myocardial fibrosis and cardiac hypertrophy, and lowered the plasma levels of creatine kinase-MB, cardiac troponin-I, and N-terminal B-type natriuretic peptide precursor in ISO-induced HF rats. It also inhibited cardiomyocyte apoptosis by upregulating B-cell lymphoma-2, downregulating Bcl-2-associated X protein, and suppressing ERS markers (glucose-related protein 78, activating transcription factor 4, and C/EBP-homologous protein). Magnesium also elevated hydrogen levels in blood, plasma, and cardiac tissue, as well as in artificial gastric juice and pure water, where hydrogen release lasted for at least four hours. Additionally, complementary *in vitro* experiments were conducted using H9C2 cardiomyocyte injury models, with hydrogen-rich culture medium as the intervention. Hydrogen-rich culture medium improved the survival and proliferation of ISO-treated H9C2 cells, reduced the cell surface area, inhibited apoptosis, and downregulated ERS pathway proteins. However, the protective effects of hydrogen were negated by tunicamycin (an inducer of ERS) in H9C2 cells. In conclusion, magnesium exerts significant cardioprotection by mitigating ERS and apoptosis through hydrogen release effects in ISO-induced HF.

Key Words: apoptosis; cardiac hypertrophy; endoplasmic reticulum stress; H9C2 cells; heart failure; hydrogen; isoproterenol; magnesium; myocardial fibrosis; rats

Introduction

Heart failure (HF) is a condition characterized by impaired heart contraction and relaxation, leading to reduced cardiac output and the body's inability to meet its physiological needs. As the end stage of many cardiovascular diseases, HF remains a leading cause of death worldwide and is often triggered by conditions such as myocarditis, arrhythmia, acute myocardial infarction, and hypertension.[1,2] A prolonged reduction in heart function disrupts both the sympathetic and humoral systems, leading to myocardial cell apoptosis, hypertrophy, and fibrosis, all of which contribute to HF progression.[3,4] Despite advancements in pharmacological treatments, such as β-adrenergic receptor antagonists and angiotensin-converting enzyme inhibitors, as well as device therapies, the incidence and mortality rates of HF remain high,[5] with epidemiological surveys indicating that 50% of HF patients die within 5 years.[6,7] These findings underscore the pressing need for therapeutic strategies targeting the underlying molecular mechanisms of HFs.

The pathogenesis of HF involves several complex molecular pathways, including apoptosis,[8] oxidative stress, endoplasmic reticulum (ER) stress (ERS),[9] and inflammatory responses.[10,11] The ER, the largest organelle in eukaryotic cells, is essential for protein synthesis, folding, transport, lipid synthesis, and calcium storage.[12] In HF, prolonged hypoxia, inflammation, and calcium imbalances disrupt protein folding, leading to ERS.[13] Cells activate unfolded protein responses to counteract ERS, attempting to restore ER homeostasis. Short-term ERS is beneficial as it signals the nucleus to reduce the number of misfolded proteins within the ER, stabilizing protein folding functions.[14,15] This adaptive mechanism is governed by three key ER transmembrane proteins: inositol-requiring enzyme 1α, protein kinase RNA-like endoplasmic reticulum kinase (PERK), and activating transcription factor 6 (ATF6).[16] Upon activation, PERK phosphorylates eukaryotic translation initiation factor 2α (eIF2α), reducing protein synthesis to alleviate ER folding pressure.[17] However, prolonged ERS shifts from protective to detrimental. Excessive activation of p-eIF2α enhances the nuclear translocation of activating transcription factor 4 (ATF4), which upregulates C/EBP-homologous protein (CHOP), initiating apoptosis through the Bcl-2 and caspase gene families and resulting in the gradual loss of myocardial cells and HF progression.[18-20] New evidence highlights the pivotal role of ERS in cardiovascular diseases. Research, such as that by Chen et al.[21] showed that ERS inhibition can reduce myocardial ischemia–reperfusion injury in rats and that similar mechanisms contribute to diabetic cardiomyopathy.[22] Given that ERS is linked to myocardial

[1]Institute of Pharmacology, Shandong First Medical University & Shandong Academy of Medical Sciences, Taian, Shandong Province, China; [2]New Drug Evaluation Center of Shandong Academy of Pharmaceutical Sciences, Shandong Academy of Pharmaceutical Sciences, Ji'nan, Shandong Province, China; [3]School of Chemistry and Pharmaceutical Engineering, Shandong First Medical University & Shandong Academy of Medical Sciences, Taian, Shandong Province, China
*__Correspondence to:__ Xiaomin Zhao, PhD, xmzhao@sdfmu.edu.cn; Rui Tan, PhD, rtan@sdfmu.edu.cn.
https://orcid.org/0000-0002-8618-8563 (Xiaomin Zhao); https://orcid.org/0009-0002-5446-0136 (Rui Tan)
#Both authors contributed equally to this work.

Funding: *This study was supported by the Pharmacology Key Discipline Foundation of Shandong Province (No. ZDXK00001) and the Collaborative Innovation Center for Research and Development of Traditional Chinese Medicine in Mount Tai (No. zd099).*
How to cite this article: *Chen F, Chen R, Yang L, Shen B, Wang Y, Gao Y, Tan R, Zhao X. Magnesium-assisted hydrogen improves isoproterenol-induced heart failure. Med Gas Res. 2025;15(4):459-470.*

hypertrophy and HF via the PERK/eIF2α/ATF4/CHOP pathway,[23] it represents a promising target for HF intervention.

Hydrogen, a colorless and odorless gas,[24] has emerged as a potential therapeutic agent.[25] First identified as protective in brain ischemia–reperfusion injury in 2007,[26] hydrogen has since shown benefits across a range of conditions, including acute renal injury, cancer, atherosclerosis, diabetes, and nervous system diseases.[27-30] These protective effects are primarily attributed to its antioxidant and anti-inflammatory properties,[25,31] along with its ability to inhibit ERS and prevent apoptosis.[32,33] Current hydrogen therapies include hydrogen-rich salt water (HRW),[34,35] hydrogen-rich nanobubble water,[36] and hydrogen–oxygen ventilators.[37] Among these, HRW has been particularly effective in reducing ERS and cell apoptosis in liver injury models.[33] Due to its high diffusibility, hydrogen can readily penetrate cell membranes, reaching key organelles to counter cellular stress.[38] Recently, magnesium-based hydrogen generators, which release hydrogen upon contact with water, have been explored for potential health applications. These generators have shown potential in improving conditions such as rheumatoid arthritis and osteoporotic bone.[39-41] However, the potential protective effects of magnesium on HF through hydrogen release remain unclear. In this study, we hypothesized that magnesium may alleviate HF via hydrogen release, which in turn reduces ERS and apoptosis. To test this hypothesis, we aimed to investigate the cardioprotective effects of magnesium and explore the mechanism linking hydrogen release, ERS, and apoptosis in a rat model of isoproterenol (ISO)-induced HF.

Materials and Methods

Preparation of HRW and hydrogen-rich culture media

HRW and hydrogen-rich culture medium (HRM) were prepared by dissolving hydrogen in physiological saline or high-glucose Dulbecco's modified Eagle medium (DMEM) using a high-purity hydrogen generator (HA300, Anjian Technology, Beijing, China) at 0.4 MPa for 4 hours. This produced a hydrogen concentration of at least 0.6 mM, as verified by a hydrogen microsensor (H2-MR-311173, Unisense, Aalborg, Denmark).[42,43] Fresh batches of HRW and HRM were prepared weekly, with diluted concentrations obtained by adjusting the saturated medium.

Animal models and treatments

To eliminate the potential impact of sex on the experiment, we used male rats as the experimental subjects. Healthy male Sprague–Dawley rats (weighing 200–220 g) were sourced from Jinan Pengyue Experimental Animal Breeding Co., Ltd. (Jinan, China, license No. SCXY (Lu) 2022 0006). They were housed under controlled conditions: 22 ± 2°C temperature, 45–60% humidity, and a 12-hour light/dark cycle, with unrestricted access to standard chow and clean water. Our experiment was approved by the Animal Care Ethics Committee of Shandong First Medical University (approval number W202303020121; dated March 3, 2023). All experiments were designed and reported according to the Animal Research: Reporting of *In Vivo* Experiments (ARRIVE) guidelines.[44]

After a 1-week acclimation period, the rats were randomly divided into nine groups (n = 5 per group): control, magnesium, ISO, ISO + Mg, ISO + magnesium chloride ($MgCl_2$), and ISO + HRW. Mg (10 mg/kg/d, Hebi Granda Magnesium Industry Co., Ltd., Hebi, China, Cat# 441010) and $MgCl_2$ (85 mg/kg/d, Solarbio, Beijing, China, Cat# M8161) were administered by gavage for 28 days, whereas the control and ISO groups received an equal volume (5 mL/kg) of physiological saline orally. HRW (10 mL/kg/d) was injected intraperitoneally for 14 days. From day 2, the above treatments were administered 1 hour before the subcutaneous injection of physiological saline (2 mL/kg) for the control and Mg groups and ISO (10 mg/kg/day, Sigma, St. Louis, Missouri, USA, Cat# 15627) for the other groups for 14 days. **Figure 1A** shows a schematic representation of the animal experimentation protocol.

At the end of 4 weeks, cardiac function was evaluated using echocardiography. The rats were anesthetized through an intraperitoneal injection of pentobarbital sodium (60 mg/kg, Sigma, Cat# 170108), and blood samples were collected from the inferior vena cava. Fresh blood was anticoagulated with heparin and centrifuged at 1000 × g for 15 minutes at 4°C to obtain plasma. The hearts were then excised, with samples either fixed in 4% paraformaldehyde for histopathological examination or snap-frozen for biochemical analysis.

Echocardiography measurement

After 4 weeks of treatment, the rats were anesthetized via inhalation of 2% isoflurane (RWD Life Science Co., Ltd., Shenzhen, China), and cardiac function was evaluated using a high-resolution ultrasound imaging system for small animals (Vevo 3100LT, Visual Sonics Inc., Tokyo, Japan). The key parameters measured included left ventricular end-systolic diameter (LVESD), left ventricular end-diastolic diameter (LVEDD), left ventricular end-systolic volume (LVESV), left ventricular end-diastolic volume (LVEDV), ejection fraction (EF), and fractional shortening (FS), all in M-mode. For each rat, the data were averaged across three cardiac cycles to ensure accuracy.

Histological analysis

Heart tissue samples were fixed in 4% paraformaldehyde, rinsed in running water for 24 hours, and dehydrated through an ethanol series of ascending concentrations. The samples were then cleared with xylene and embedded in paraffin. Sections (4 μm in thickness) were prepared and stained with hematoxylin-eosin (Cat# G1120, Solarbio) and Masson's trichrome stain (Cat# G1346, Solarbio) according to the manufacturer's instructions. Stained sections were examined using a digital pathology scanning system (Pannoramic Scan, 3DHISTECH, Budapest, Hungary).

Plasma biochemical analysis

The plasma levels of creatine kinase (CK-MB), cardiac troponin (cTn-I), and N-terminal B-type natriuretic peptide precursor (NT-proBNP) were detected using enzyme-linked immunosorbent assay kit (Shanghai Yuanju Biotechnology, Shanghai, China) following the manufacturer's instructions.

Cell culture and treatment

H9C2 cells (Cat# CL-0089, RRID: CVCL_0286) from Procell Life Science & Technology Co., Ltd. (Wuhan, China) were cultured in high-glucose DMEM supplemented with 10% fetal bovine serum and 1% penicillin–streptomycin. The medium was changed every 3 days, and the cells were maintained at 37°C with 5% CO_2 until they reached 80–90% confluence. The experimental groups included the following: control: H9C2 cells were consistently cultured in DMEM complete medium; ISO: after H9C2 cells were cultured in DMEM complete medium for 24 hours, they were incubated with ISO (25 μg/mL) for 24 hours, then washed three times with phosphate buffered saline (PBS) and cultured in fresh medium for 12 hours; ISO + HRM (15, 50, 150 μM): after H9C2 cells were pretreated with 15, 50, or 150 μM HRM for 24 hours, they were washed with PBS three times, incubated with ISO (25 μg/mL) for 24 hours, again washed with PBS three times, and cultured in fresh medium for 12 hours; and ISO + 150 μM HRM + tunicamycin: after H9C2 cells were pretreated with 150 μM HRM for 24 hours, they were washed three times with PBS, incubated with ISO (25 μg/mL) for 24 hours, again washed three times with PBS, and treated with 5 μg/mL tunicamycin (dissolved in dimethyl sulfoxide, Cell Signaling, Danvers, MA, USA, Cat# CL-12819S) for 12 hours. Except for the ISO + 150 μM HRM + tunicamycin group, the remaining groups were treated with 2 μL of dimethyl sulfoxide for 12 hours. **Figure 1B** illustrates the procedural flowchart for the cellular experiment.

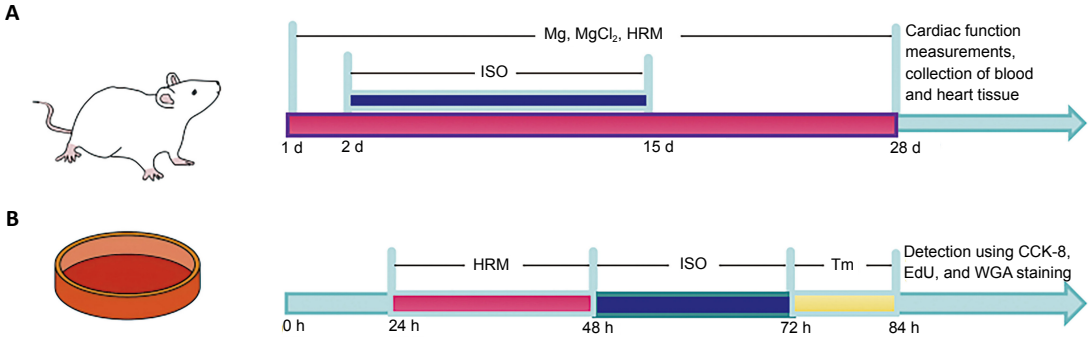

Figure 1 | Flow chart of the animal and cell experiments.
(A) Animal experiment flowchart. The purple area represents the time during which the magnesium, $MgCl_2$, and HRW treatments were administered, and the blue area represents the period during which ISO subcutaneous injection induced HF. (B) Flowchart of the cell experiment. The purple area represents pretreatment with HRM for 24 hours, the blue area represents ISO treatment for 24 hours, and the yellow area represents treatment with tunicamycin for 12 hours. CCK-8: Cell Counting Kit-8; EdU: 5-ethynyl-2′-deoxyuridine; HRM: hydrogen-rich culture medium; HRW: hydrogen-rich saltwater; ISO: isoproterenol; $MgCl_2$: magnesium chloride; Tm: tunicamycin; WGA: wheat germ agglutinin.

Wheat germ agglutinin staining

For cardiac tissue staining, the sections were dewaxed, rehydrated, and incubated with wheat germ agglutinin (10 mg/mL, Cat# W1126, Invitrogen, Carlsbad, CA, USA) for 30 minutes in the dark. The slides were then washed three times with PBS and sealed with antifade mounting medium before being observed under a fluorescence microscope (DM4000B, Leica, Wetzlar, Germany).

For H9C2 cell staining, drug-treated cells were washed twice with fresh culture medium and fixed with immunostaining fixative (Cat# p0098, Beyotime, Shanghai, China) for 30 minutes. Afterward, they were incubated with wheat germ agglutinin reaction solution at room temperature for 25 minutes in the dark, counterstained with 4′,6-diamidino-2-phenyllndole, and observed under a fluorescence microscope.

Terminal dUTP nick end labeling

Apoptosis in cardiac tissue was assessed using a one-step terminal dUTP nick end labeling (TUNEL) cell apoptosis detection kit (Cat# C1088, Beyotime). Heart tissues embedded in paraffin were sectioned into 4 µm slices. Following dewaxing and rehydration, the sections were incubated with TUNEL reaction solution at 37°C in the dark for 1 hour. After incubation, the sections were rinsed with PBS, sealed with antifade mounting medium containing 4′,6-diamidino-2-phenylindole, and examined under a fluorescence microscope.

For the cell-based experiments, the drug-treated cells were first rinsed twice with fresh culture medium and then fixed with immunostaining fixative for 30 minutes. The cells were subsequently processed in the same manner as those in the cardiac tissue sections.

Detection of hydrogen and Mg^{2+} concentrations

Hydrogen levels in the blood, plasma, artificial gastric juice, pure water, and cardiac tissue homogenate were measured using a hydrogen microsensor (H2-MR-311173, Unisense, Aalborg, Denmark; 50 nM of the detection limit for hydrogen concentration; 0–800 µmol of the measurement range for hydrogen concentration) connected with a pico ammeter (PA2000, Unisense).[45-49]

For the *in vitro* hydrogen release experiments, 1 mL of artificial gastric juice (1.64% hydrochloric acid, 1% gastric protease, pH 1.3) or pure water was mixed with different magnesium masses (0.01, 0.03, 0.1, 0.3, or 1 mg) in a microrespiration chamber at 37°C. A rotor was added, and the speed was adjusted to 600 r/min. The microsensor was inserted into the microrespiration chamber through the cap hole to detect the hydrogen concentration. When the hydrogen concentration in the blood was detected, 1 mL of fresh heparin-anticoagulated blood was quickly transferred to a microrespiration chamber, and the microsensor was used to detect the hydrogen level. The plasma was prepared via centrifugation of sealed heparin-anticoagulated blood. Cardiac homogenate was obtained after fresh cardiac tissue was homogenized with physiological saline (mass-to-volume ratio of 100 mg/mL). Then, the plasma and cardiac homogenate were quickly added into a microrespiration chamber, and hydrogen levels were detected using the abovementioned method.

Additionally, plasma Mg^{2+} levels were measured using a magnesium ion assay kit (Cat# c005-1-1, Nanjing Jiancheng Bioengineering Institute, Nanjing, China) with absorbance at 540 nm using a microplate reader (Infinite 200 pro, TECAN, Vienna, Austria).

Cell viability assay

Cell viability was measured sing the Cell Counting Kit-8 (CCK-8) (Cat# CT0001-B; SparkJade, Qingdao, China) according to the manufacturer's instructions. H9C2 cells (8000 per well) were seeded in 96-well plates, treated as per the experimental design, washed twice with high-glucose DMEM, and incubated with 10 µL of CCK-8 reagent per well at 37°C with 5% CO_2 for 2 hours. The absorbance was measured at 450 nm using a microplate reader (Infinite 200 PRO, TECAN).

5-Ethynyl-2′-deoxyuridine staining

For proliferation analysis, H9C2 cells (8000 per well) were seeded in 96-well plates and incubated for 24 hours. 5-Ethynyl-2′-deoxyuridine (EdU) staining was conducted with a BeyoClick™ EdU cell proliferation assay kit (Cat# C0071S, Beyotime). Following treatment, the medium was replaced with fresh medium containing 10 µM EdU. The cells were incubated for 2 hours, fixed with 4% paraformaldehyde for 15 minutes, washed, and stained with the reaction mixture according to the kit instructions; then, the cells were counterstained with Hoechst 33342 and observed under a fluorescence microscope.

Western blotting

Total protein from rat heart tissue and H9C2 cells was extracted using RIPA lysis buffer (Cat# R0010, Solarbio) containing a protein phosphatase inhibitor (Cat# P1260, Solarbio). Protein concentrations were determined using a bicinchoninic acid assay (Cat# PC0020; Solarbio). Proteins were separated by 10% sodium dodecyl sulfate–polyacrylamide gel electrophoresis and transferred to polyvinylidene fluoride membranes. The membranes were blocked with 5% skim milk in Tris-buffered saline with Tween-20 for 4 hours at room temperature (22 ± 2°C) and then incubated overnight at 4°C with

primary antibodies against Bcl-2 (rabbit, 1:1000, Abcam, Cambridge, UK, Cat# ab196495, RRID: AB_2924862), Bax (rabbit, 1:1000, Abcam, Cat# ab32503, RRID: AB_725631), glucose-related protein78 (GRP78; rabbit, 1:1000, Abcam, Cat# ab108613, RRID: AB_10859806), ATF4 (rabbit, 1:1000, Abcam, Cat# ab216839, RRID: AB_3676365), cardiac troponin I (cTn-I; rabbit, 1:1000, Abcam, Cat# ab209809, RRID: AB_2890981), phosphorylated cTn-I (p-cTn-I; rabbit, 1:1000, Abcam, Cat# ab190697, RRID: AB_3676364), CHOP (mouse, 1:1000, Cell Signaling, Cat# 2895, RRID: AB_2089254) and glyceraldehyde-3-phosphate dehydrogenase (GAPDH; rabbit, 1:10,000, Abcam, Cat# ab181602, RRID: AB_2630358).The membranes were then washed and incubated for 1 hour at 22 ± 2°C with secondary antibodies of goat anti-rabbit IgG (1:3000, Servicebio, Wuhan, China, Cat# GB23301, RRID: AB_2904020) or goat anti-mouse IgG (1:3000, Servicebio, Cat# GB23303, RRID: AB_2811189) and visualized via an enhanced chemiluminescence (ECL) reagent (Cat#1810202, Clinx, Shanghai, China) and a chemiluminescence imaging system (Amersham imager 600, Tanon, Shanghai, China). Band intensity was quantified via ImageJ-win64 software (National Institutes of Health, Bethesda, MD, USA).[50]

Statistical analysis

The sample size calculation for *in vivo* experiments was performed as follows: Based on the study design and groupings, one-way analysis of variance was chosen as the statistical test. After the significance level and statistical power were set, the effect size and within-group variability were estimated from our pilot experiments. Using these estimates, we then calculated the minimum required sample size. The evaluators were blinded to the groupings, with the exception of the first and corresponding authors. The experiment was conducted in three separate batches, with the sample size ultimately maintained. In total, two rats died in both the ISO and ISO + $MgCl_2$ (85 mg/kg) groups, whereas one rat died in each of the ISO + Mg (0.3 mg/kg), ISO + Mg (3 mg/kg), and ISO + HRW (10 mL/kg) groups.

The data are presented as the mean ± standard error of the mean (SEM). For the *in vitro* hydrogen release experiment, two-way analysis of variance was used to analyze differences among groups at various time points. Other group differences were analyzed using one-way analysis of variance followed by Tukey's post hoc test for multiple comparisons, and correlation analysis of two variables was conducted via linear regression, with statistical significance set at $P < 0.05$. Analyses were performed with GraphPad Software (version 8.4.0; GraphPad Software, San Diego, CA, USA; www.graphpad.com).

Results

Magnesium improves cardiac function in ISO-induced HF model rats

Using echocardiography, we assessed the cardioprotective effects of magnesium in HF models. Key measures, including EF, FS, LVEDV, LVESV, LVEDD, and LVESD, were evaluated to track cardiac function. Compared with the control group, the heart failure model (ISO) group presented significant reductions in EF and FS, alongside notable increases in LVEDV, LVESV, LVEDD, and LVESD, indicating impaired cardiac function. Treatment with magnesium and HRW notably improved these parameters, as EF and FS increased, whereas LVEDD, LVESD, LVESV, and LVEDV decreased (**Figure 2A–G**). In contrast, $MgCl_2$ treatment had no significant effect on cardiac function.

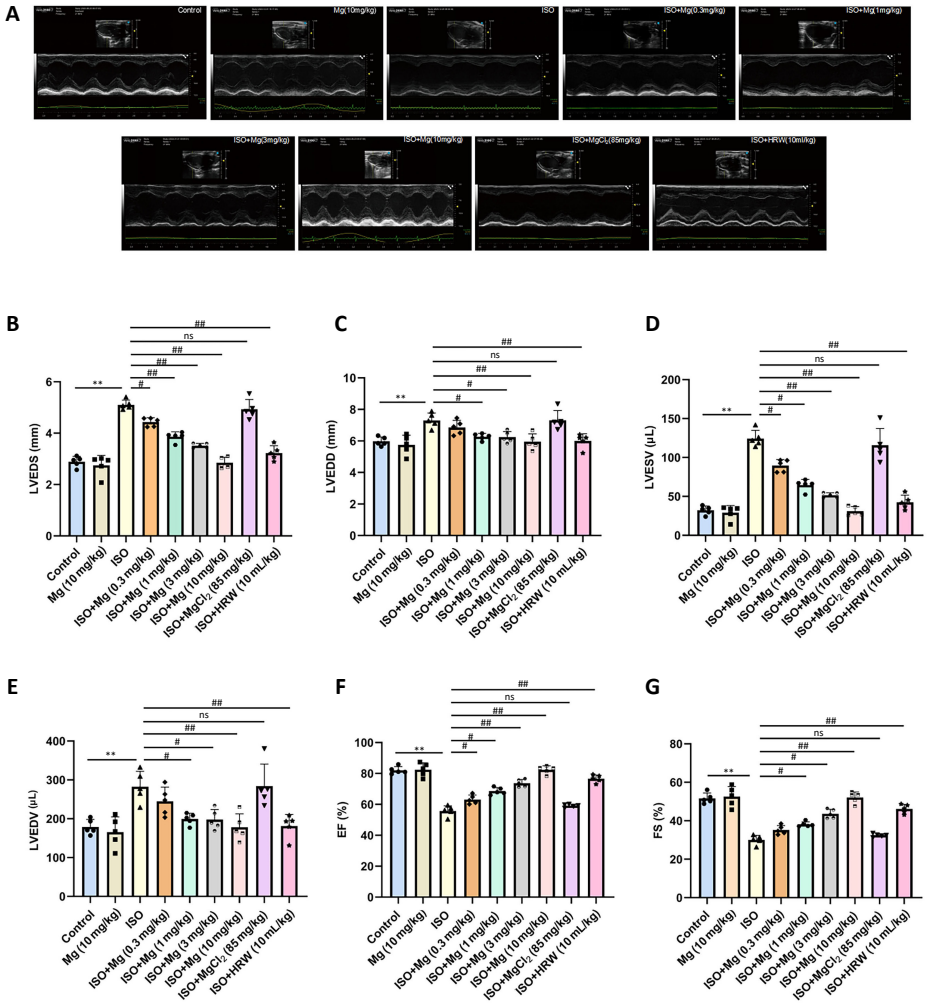

Figure 2 | Magnesium ameliorates cardiac function in ISO-induced heart failure in rats.
(A) Representative echocardiographic images. Rats in the ISO group exhibited cardiac dysfunction, whereas treatment with magnesium and HRW significantly improved cardiac function. (B–G) Changes in LVESD (B), LVEDD (C), LVESV (D), LVEDV (E), EF (F), and FS (G) from echocardiographic measurements. The data are expressed as the mean ± SEM (n = 5). $^{**}P < 0.01$, *vs*. the control group; $^{\#}P < 0.05$, $^{\#\#}P < 0.01$, *vs*. the ISO group (one-way analysis of variance followed by Tukey's *post hoc* test). EF: Ejection fraction; FS: functional shortening; HRW: hydrogen-rich saltwater; ISO: isoproterenol; LVEDD: left ventricular end-diastolic diameter; LVESD: left ventricular end-systolic diameter; LVEDV: left ventricular end-diastolic volume; LVESV: left ventricular end-systolic volume; Mg: magnesium; $MgCl_2$: magnesium chloride.

Magnesium reduces myocardial hypertrophy and fibrosis in ISO-induced HF rats

Histopathological analysis further revealed the impact of magnesium on cardiac tissue. Myocardial hypertrophy, a hallmark of heart failure,[51] was measured via wheat germ agglutinin staining, which revealed significant enlargement of myocardial cells in the model group. Magnesium and HRW effectively reduced the cell size, whereas $MgCl_2$ had no effect (**Figure 3A** and **B**).

Furthermore, magnesium and HRW reduced the HW/BW, LVW/BW, and LVW/TL ratios (**Figure 3C–E**), further confirming the reduction in hypertrophy. Hematoxylin–eosin staining revealed inflammatory cell infiltration and disordered arrangement of myocardial cells in the heart tissue of ISO-treated rats. Magnesium and HRM alleviated this damage to varying degrees (**Figure 3F**). Masson staining revealed increased collagen deposition (fibrosis) in the ISO-treated rats, which was also reduced with magnesium and HRW treatments (**Figure 3G** and **H**). Additionally, the levels of plasma myocardial damage markers (CK-MB, cTn-I, and NT-proBNP) were significantly decreased by magnesium and HRW but remained unaffected by $MgCl_2$ (**Figure 3I–K**). In addition, western blot was used to measure the levels of p-cTn-I in cardiac tissue and demonstrated that magnesium and HRM significantly decreased the levels of p-cTn-I (**Figure 3L** and **M**). These results support the tissue-protective role of magnesium, unlike $MgCl_2$.

Magnesium inhibits apoptosis and ERS in ISO-induced HF rats

To assess cardiac cell apoptosis, TUNEL staining was performed. Compared with the control group, the HF model group presented a marked increase in myocardial cell apoptosis. However, treatment with magnesium and HRW significantly reduced apoptosis, whereas $MgCl_2$ had no noticeable effect (**Figure 4A** and **B**). Western blot analysis was used to further investigate the levels of apoptosis-related proteins. In the ISO-induced group, there was an increase in the protein expression of Bax and a decrease in the protein expression of Bcl-2, both of which are key markers of apoptosis.[52] Treatment with magnesium and HRW inhibited Bax protein expression while promoting Bcl-2 protein expression, effectively mitigating apoptosis (**Figure 4C–E**). The ERS was subsequently evaluated. In ISO-induced HF rats, ERS markers—GRP78, ATF4, and CHOP—were significantly elevated. Magnesium and HRW treatment markedly reduced the expression of these stress markers, whereas $MgCl_2$ had no such effect (**Figure 4F–I**). These findings suggest that magnesium treatments help alleviate apoptosis and ER stress, highlighting their potential cardioprotective effects.

Magnesium releases hydrogen *in vitro* and *in vivo*, which is correlated with HF parameters

To determine whether magnesium can release hydrogen in the stomach when delivered via the gastrointestinal tract, we measured hydrogen concentrations following the introduction of magnesium into artificial gastric juice and pure water. Our results revealed that hydrogen levels were significantly higher in both groups than in the control group, with elevated concentrations persisting for over four hours (**Figure 5A** and **B**). To further explore the potential of magnesium for *in vivo* hydrogen release, we measured hydrogen levels in the blood, plasma, and heart tissue. Compared with ISO-treated rats, magnesium-treated rats presented significantly higher hydrogen concentrations in all three samples. In contrast, $MgCl_2$ did not exhibit similar increases (**Figure 5C–E**). Additionally, magnesium treatment elevated plasma Mg^{2+} levels (**Figure 5F**), suggesting that oral magnesium reacts with stomach acid to release hydrogen within the body.

Linear regression analysis revealed that plasma hydrogen levels were positively correlated with EF ($r = 0.81$, $P < 0.01$) and negatively correlated with both the collagen volume fraction (CVF) ($r = 0.73$, $P < 0.01$) and the myocardial cell cross-sectional area (MCCA) ($r = 0.79$, $P < 0.01$) (**Figure 5G–I**). However, no significant correlations were detected between plasma Mg^{2+} levels and EF ($r = 0.26$, $P = 0.09$), CVF ($r = 0.11$, $P = 0.17$), or MCCA ($r = 0.15$, $P = 0.33$) (**Figure 5J–L**). These findings indicate that the cardioprotective effects observed in magnesium-treated, ISO-induced HF rats are more likely due to hydrogen than Mg^{2+}.

Hydrogen ameliorates ISO-induced damage to H9C2 cardiomyocytes

To strengthen our *in vivo* findings, we conducted *in vitro* experiments using HRM as an intervention to assess its effects on ISO-induced injury in H9C2 cardiomyocytes. Initially, the toxicity of HRM and ISO on H9C2 cells was evaluated by exposing the cells to various concentrations of HRM (15, 50, or 150 μM) and ISO (6.25, 12.5, or 25 μg/mL) for 24 hours, and cell viability was measured via the CCK-8 assay. The results indicated that HRM, at all the tested concentrations, did not significantly affect cell viability (**Figure 6A**). However, ISO (12.5 and 25 μg/mL) significantly reduced cell survival (**Figure 6B**), leading us to select the higher concentration of 25 μg/mL ISO for subsequent experiments to model H9C2 cardiomyocyte injury.

Further analysis demonstrated that pretreatment with HRM markedly improved the viability of ISO-treated H9C2 cells in a dose-dependent manner (**Figure 6C**). Additionally, EdU staining revealed that, compared with the control, ISO treatment substantially inhibited H9C2 cell proliferation, whereas HRM pretreatment significantly restored the proliferative capacity (**Figure 6D** and **E**). HRM also reduced the surface area of ISO-treated cells, indicating a protective effect against hypertrophy (**Figure 6F** and **G**). Collectively, these findings suggest that HRM mitigates ISO-induced damage to and hypertrophy in H9C2 cardiomyocytes.

Hydrogen reduced ISO-induced apoptosis and ERS in H9C2 cells

In vitro, we investigated the effect of HRM on ISO-induced apoptosis in H9C2 cells via TUNEL staining. ISO treatment significantly increased apoptosis, which was notably reduced by HRM pretreatment. However, this protective antiapoptotic effect was negated when tunicamycin, an inducer of ERS, was introduced (**Figure 7A** and **B**). Further analysis via western blot revealed that HRM lowered Bax levels and enhanced Bcl-2 expression in ISO-treated cells, reinforcing its antiapoptotic properties (**Figure 7C–E**). We reintroduced tunicamycin to explore whether the antiapoptotic effect of HRM involved ERS inhibition. Consistent with previous findings, Western blot analysis revealed that HRM markedly reduced the expression of the ERS-related proteins GRP78, ATF4, and CHOP in ISO-treated H9C2 cells. However, this effect was reversed by tunicamycin (**Figure 7F–I**). These results suggest that HRM alleviates ISO-induced apoptosis by suppressing ERS.

Discussion

This study demonstrated that magnesium, acting as a hydrogen donor, substantially enhances cardiac function in rats with ISO-induced HF, as evidenced by reduced plasma levels of CK-MB, cTn-I, and NT-proBNP, along with decreased cardiomyocyte hypertrophy and fibrosis. Consistent with these *in vivo* findings, *in vitro* studies on ISO-induced H9C2 cardiomyocytes revealed that hydrogen improves cell survival and proliferation, reduces cell size, and inhibits apoptosis by suppressing ERS.

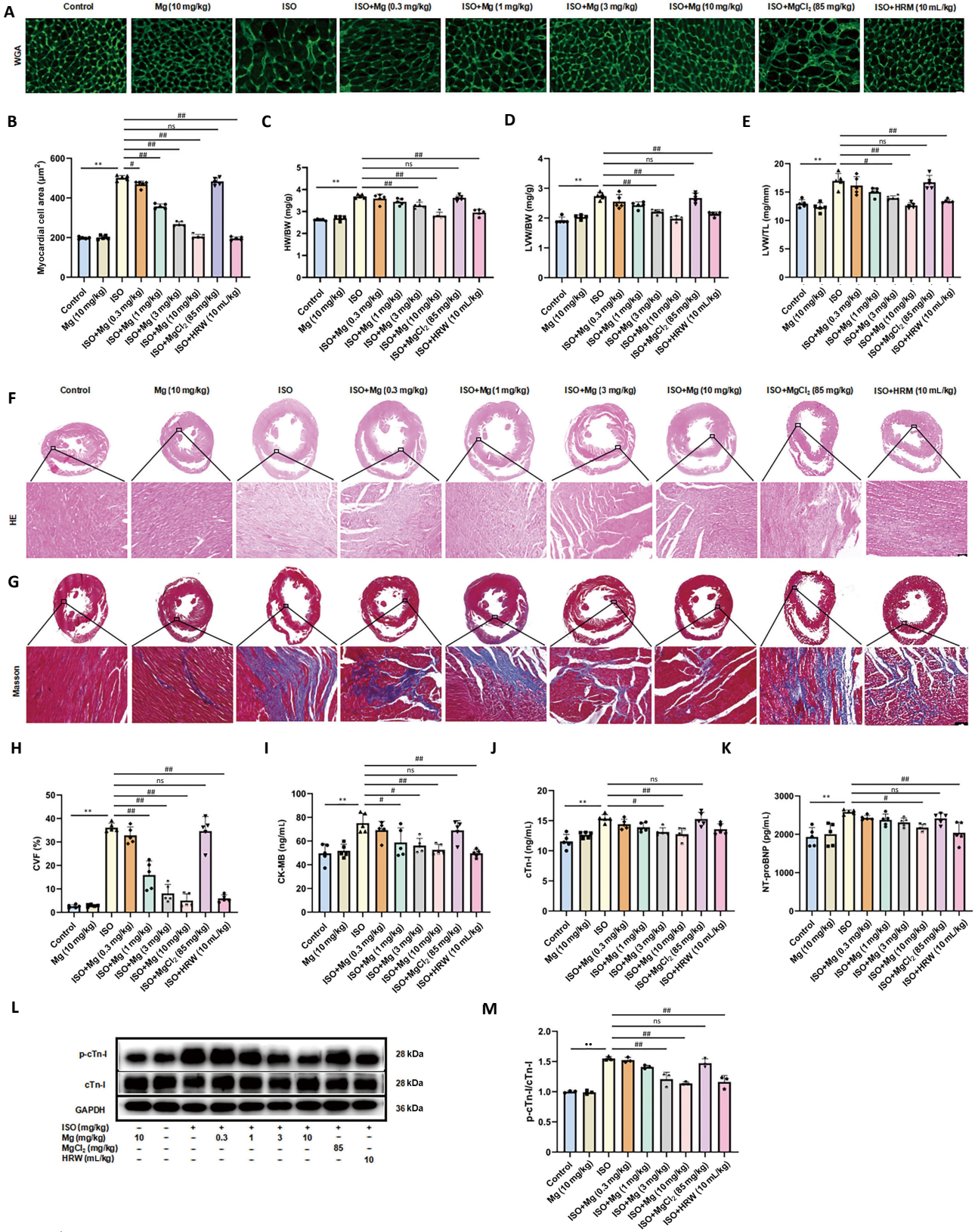

Figure 3 | Magnesium alleviates myocardial hypertrophy and fibrosis in ISO-induced heart failure in rats.

(A) Representative WGA staining of heart tissues. ISO group rats showed significant enlargement of myocardial cells, and magnesium and HRW effectively reduced the cell size. Scale bar: 20 μm. (B) Myocardial cell cross-sectional area. (C–E) Ratios of HW/BW (C), LVW/BW (D), and LVW/TL (E). (F) Representative HE staining of heart tissues (n = 3). Inflammatory cell infiltration and disordered arrangement of myocardial cells were observed in the heart tissue of ISO group rats, and magnesium and HRM alleviated this damage. Scale bar: 100 μm. (G) Representative Masson staining of heart tissues, where blue indicates collagen. Collagen deposition in the myocardium of ISO-treated rats significantly increased, but it was also reduced with magnesium and HRW treatments. Scale bar: 100 μm. (H) Quantification of myocardial fibrosis areas. (I–K) Plasma levels of CK-MB (I), cTn-I (J), and NT-proBNP (K). (L) Immunoblots of p-cTn-I and cTn-I proteins. (M) Quantification of p-cTn-I/cTn-I (n = 3). The data are expressed as the mean ± SEM (n = 5). $^{**}P < 0.01$, *vs.* the control group; $^{\#\#}P < 0.05$, $^{\#\#}P < 0.01$, *vs.* the ISO group (one-way analysis of variance followed by Tukey's *post hoc* test). BW: Body weight; CK-MB: creatine kinase-MB; cTn-I: cardiac troponin-I; CVF: collagen volume fraction; GAPDH: glyceraldehyde-3-phosphate dehydrogenase; HE: hematoxylin-eosin; HRW: hydrogen-rich saltwater; HW: heart weight; ISO: isoproterenol; LVW: left ventricular weight; MCCA: myocardial cell cross-sectional area; Mg: magnesium; $MgCl_2$: magnesium chloride; NT-proBNP: N-terminal B-type natriuretic peptide precursor; p-cTn-I: phosphorylated cardiac troponin-I; TL: tibial length; WGA: wheat germ agglutinin.

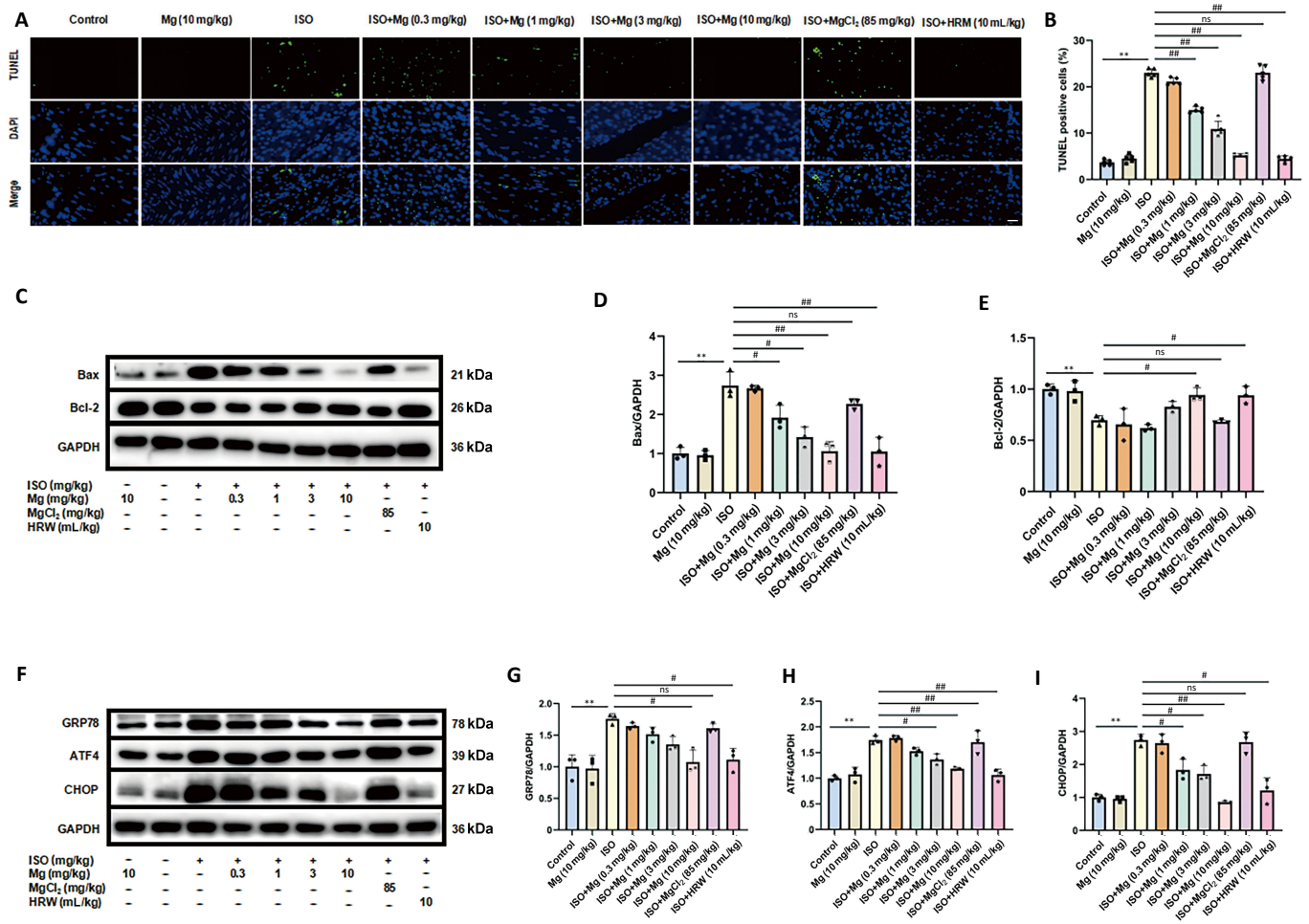

Figure 4 | Magnesium suppresses apoptosis and ERS in ISO-induced heart failure in rats.
(A) TUNEL staining (green) of heart tissues counterstained with DAPI (blue) (n = 5). The ISO group presented a significant increase in myocardial cell apoptosis, which was markedly reduced with magnesium and HRW treatments. Scale bar: 100 μm. (B) Percentage of TUNEL-positive cells. (C) Immunoblots of the Bax and Bcl-2 proteins. (D, E) Quantification of Bax (D) and Bcl-2 (E) expression. (F) Immunoblots of GRP78, ATF4, and CHOP. (G–I) Quantification of GRP78 (G), ATF4 (H), and CHOP (I) protein expression. The data are expressed as the mean ± SEM (n = 3). *P < 0.05, **P < 0.01, *vs*. the control group; #P < 0.05, ##P < 0.01, *vs*. the ISO group (one-way analysis of variance followed by Tukey's *post hoc* test). ATF4: Activating transcription factor 4; Bax: Bcl-2 associated X protein; Bcl-2: B-cell lymphoma-2; CHOP: C/EBP-homologous protein; DAPI: 4',6-diamidino-2-phenylindole; GAPDH: glyceraldehyde-3-phosphate dehydrogenase; GRP78: glucose-related protein78; HRW: hydrogen-rich saltwater; ISO: isoproterenol; Mg: magnesium; $MgCl_2$: magnesium chloride; TUNEL: terminal dUTP nick end labeling.

ISO, a β-adrenergic receptor agonist,[53] initially increases heart rate and myocardial contractility. However, long-term β-receptor activation can lead to the transformation of myocardial fibroblasts into myofibroblasts, increased production of extracellular matrix (such as collagen), and the development of myocardial fibrosis.[54] The mechanism underlying ISO-induced cardiac injury is also linked to its elevation of oxygen-free radicals.[55] Oxidative stress has been recognized as a key trigger for myocardial hypertrophy, and prolonged pathological hypertrophy typically leads to a decline in cardiac contractile function.[56] Additionally, oxidative stress can induce cell apoptosis through various pathways, including inflammatory responses. Together, these factors push the heart from a compensatory state to a decompensated state, contributing to the progression of HF.[57] In the ISO-induced HF model, biomarkers such as cTn and NT-proBNP are elevated,[58] reflecting the pathological processes observed in human HF.[59-61] Biomarkers such as CK-MB, cTn-I, and NT-proBNP are well-established indicators of HF.[62-64] Prior studies have successfully induced HF in rats through subcutaneous ISO injection, resulting in impaired cardiac function, increased collagen synthesis, and cardiomyocyte hypertrophy.[65,66] Our study revealed similar significant cardiac dysfunction and elevated myocardial damage, hypertrophy, and fibrosis markers, validating our HF model.

Using this ISO-induced HF model, we found that magnesium treatment markedly improved cardiac function, reduced myocardial hypertrophy and fibrosis, and lowered plasma biomarker levels, confirming its cardioprotective effects. Given that orally administered magnesium reacts with stomach acid and water in the digestive tract to release both Mg^{2+} and hydrogen,[67] we sought to determine whether these cardioprotective effects of magnesium were attributable to Mg^{2+} or hydrogen. We administered $MgCl_2$ at a dose (85 mg/kg) equivalent to the amount of Mg^{2+} released by the highest dose of magnesium (10 mg/kg), which did not improve heart function, fibrosis, hypertrophy, or biomarker levels. Although Mg^{2+} has proven beneficial for certain cardiac conditions, such as arrhythmia,[68] ischemia–reperfusion injury,[69] and diabetic cardiomyopathy,[70] clinical studies have shown no correlation between Mg^{2+} levels and HF outcomes.[71] Additionally, intravenous injection of Mg^{2+} does not affect HFs in clinical settings,[72] which aligns with our findings. Moreover, our studies revealed that plasma Mg^{2+} levels did not correlate with EF, CVF, or MCCA. These findings suggest that Mg^{2+} is not the primary driver of magnesium's protective effect against HF.

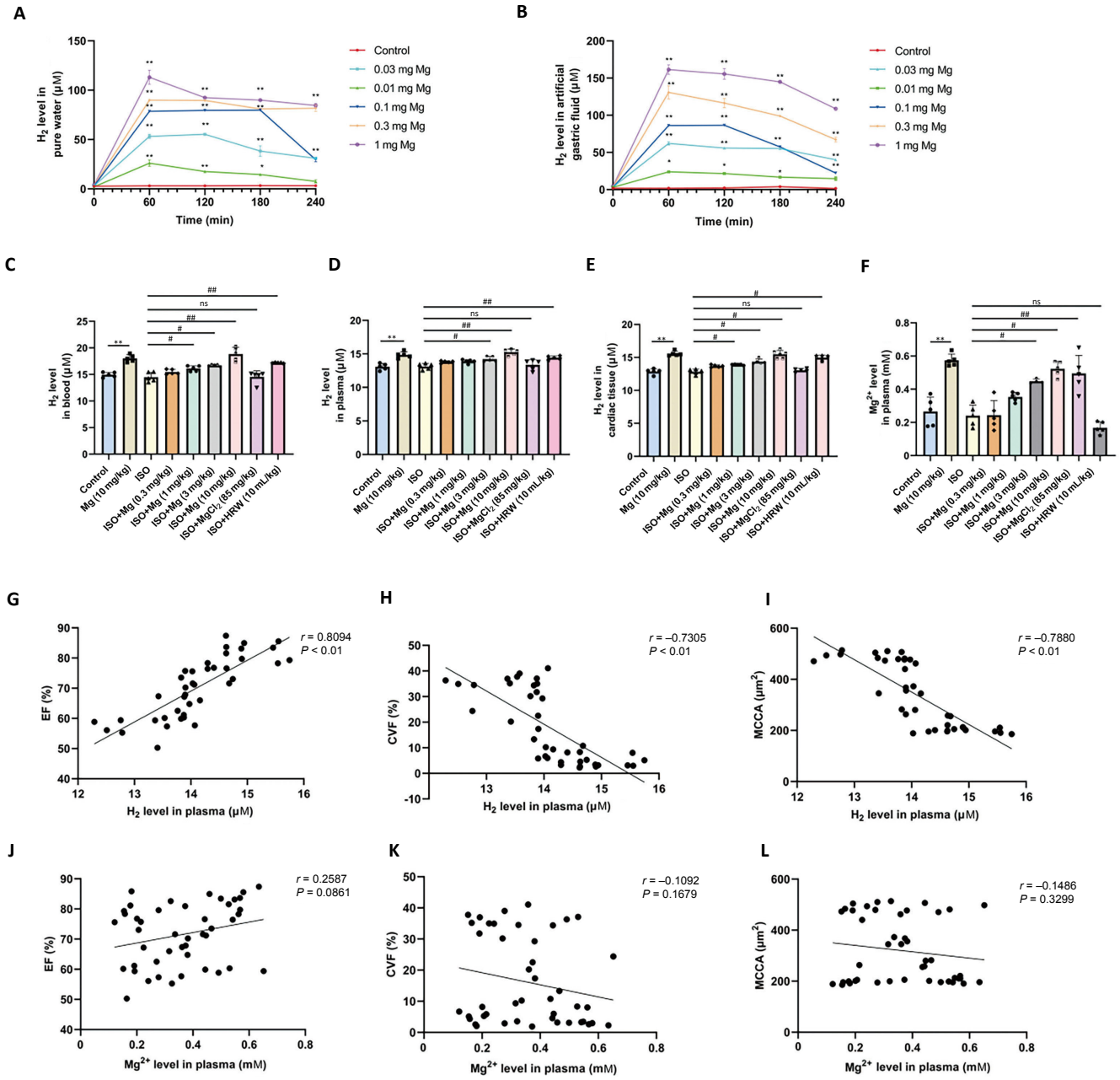

Figure 5 | **Magnesium releases hydrogen *in vitro* and *in vivo*, which is correlated with heart failure parameters.**
(A, B) Hydrogen is released by magnesium in artificial gastric fluid and pure water (n = 3). (C–E) Hydrogen levels in rat blood (C), plasma (D), and heart tissues (E). (F) Plasma Mg^{2+} levels. The data are expressed as the mean ± SEM (n = 4–5). *P < 0.05, **P < 0.01, *vs*. the control group; #P < 0.05, ##P < 0.01, *vs*. the ISO group (two-way analysis or one-way analysis of variance followed by Tukey's *post hoc* test). (G–I) Correlations of plasma hydrogen with EF (G), CVF (H), and MCCA (L). (J–L) Correlations of plasma Mg^{2+} levels with EF (J), CVF (K), and MCCA (L). CVF: Collagen volume fraction; EF: ejection fraction; HRW: hydrogen-rich saltwater; ISO: isoproterenol; MCCA: myocardial cell cross-sectional area; Mg: magnesium; $MgCl_2$: magnesium chloride.

Since Mg^{2+} did not account for the observed protective effect, we hypothesized that the hydrogen released from oral magnesium might contribute to these cardioprotective effects. To investigate this, we measured hydrogen levels across several samples, including blood, plasma, heart tissue, artificial gastric juice, and pure water, through both *in vivo* and *in vitro* experiments. Our findings revealed that various doses of magnesium increased the hydrogen concentration in these samples, whereas $MgCl_2$ did not produce similar increases. Additionally, we observed a strong correlation between plasma hydrogen levels and measures of HF, such as EF, CVF, and MCCA. These findings, along with *in vivo* evidence of the protective effects of hydrogen being comparable to those of magnesium, suggest that hydrogen may be a key factor in the cardioprotective effect of magnesium in HF.

To explore this further, we conducted *in vitro* experiments using HRM at concentrations of 15, 50, and 150 μM, selecting the minimum HRM concentration on the basis of the average hydrogen concentration observed in the heart tissue of rats treated with ISO and magnesium. These trials aimed to determine whether hydrogen released from magnesium could protect against cardiomyocyte damage in HF. We induced injury in H9C2 cells via ISO, confirming previous findings by Liao et al.[66] and Song et al.[73] in which ISO significantly reduced survival and proliferation while increasing the surface area of H9C2 cardiomyocytes. We found that HRM treatment improved the survival and proliferation of ISO-treated H9C2 cells and reduced the cell surface area, demonstrating a clear cardioprotective effect.

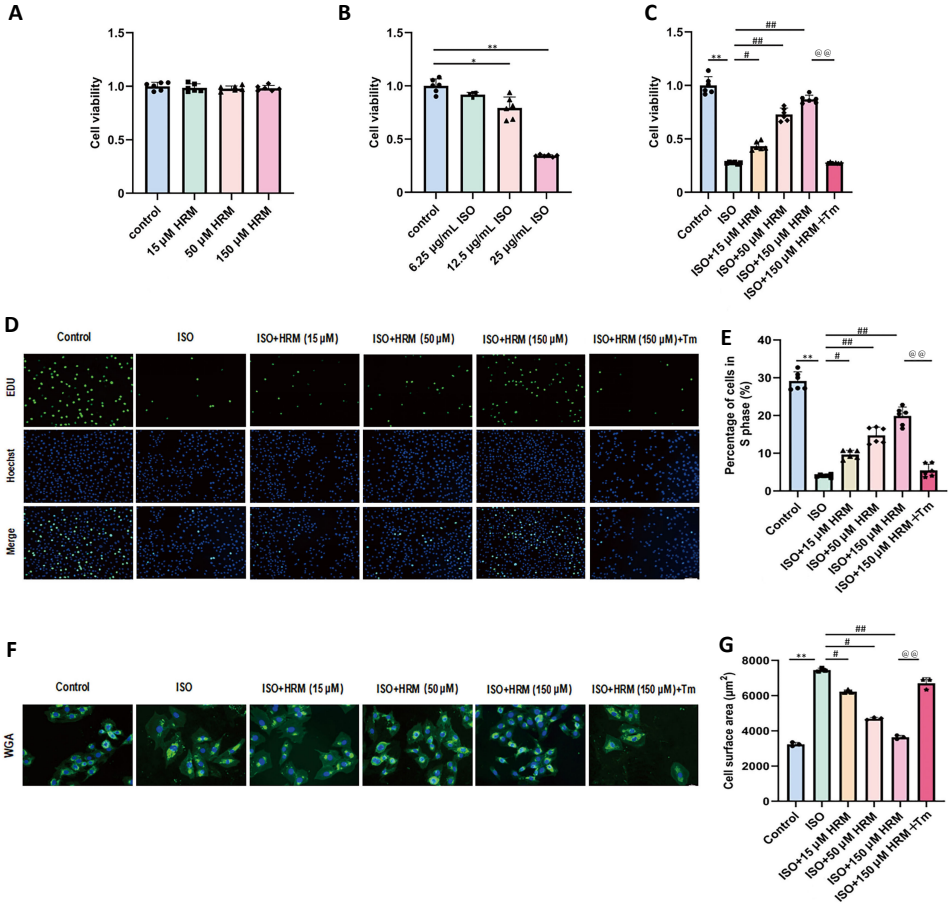

Figure 6 | Hydrogen mitigates ISO-induced damage to H9C2 cardiomyocytes. (A–C) CCK-8 assay showing the effects of HRM and ISO on H9C2 cell viability. (D) EdU (green) and Hoechst (blue) staining of H9C2 cells (n = 6). The proliferation of cells in the ISO group was significantly reduced, whereas HRW treatment increased the proliferation of ISO-induced H9C2 cells. Scale bar: 100 μm. (E) Quantitative analysis of EdU incorporation. (F) WGA staining (green) with DAPI counterstaining (blue) (n = 3). The cells in the ISO group exhibited hypertrophy, while HRW treatment reduced their surface area. Scale bar: 20 μm. (G) Quantitative analysis of WGA staining. The data are expressed as the mean ± SEM. *P < 0.05, **P < 0.01, vs. the control group; #P < 0.05, ##P < 0.01, vs. the ISO group; $^{@@}P$ < 0.01, vs. the ISO + 150 μM HRM + tunicamycin group (one-way analysis of variance followed by Tukey's $post\ hoc$ test). CCK-8: Cell Counting Kit-8; EDU: 5-ethynyl-2′-deoxyuridine; HRM: hydrogen-rich culture medium; ISO: isoproterenol; Mg: magnesium; $MgCl_2$: magnesium chloride; Tm: tunicamycin; WGA: wheat germ agglutinin.

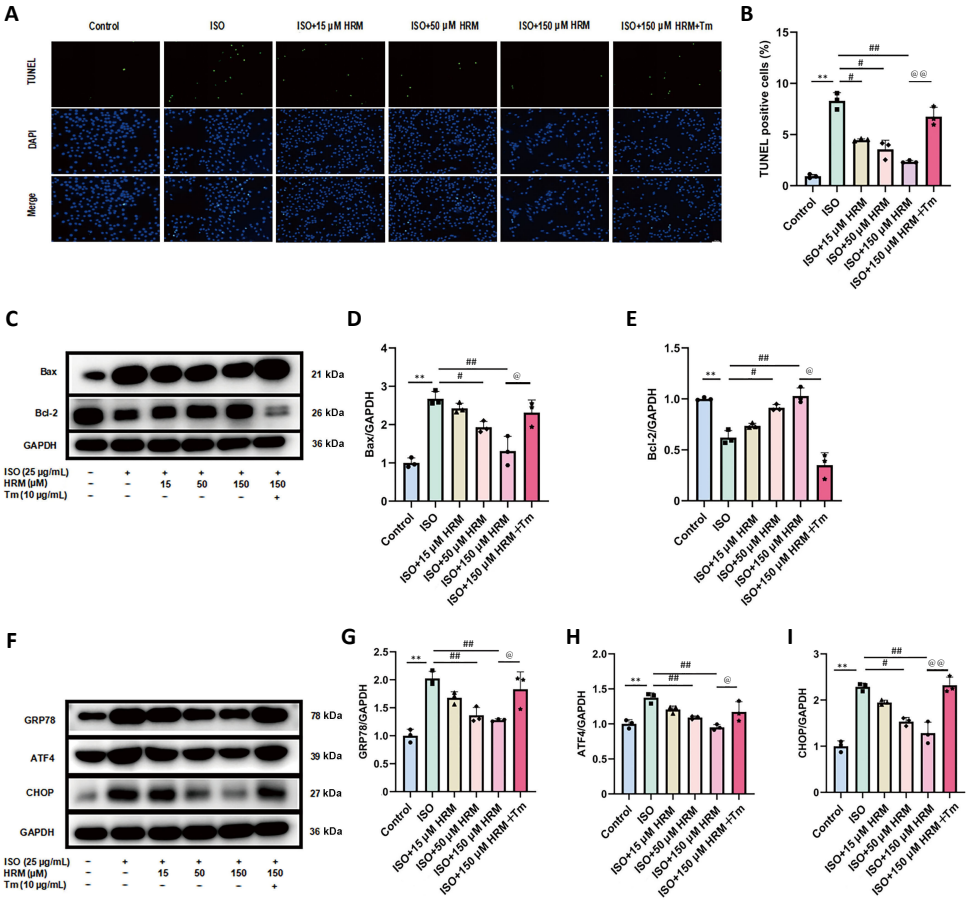

Figure 7 | Hydrogen inhibits ISO-induced apoptosis and ERS in H9C2 cells. (A) TUNEL staining of H9C2 cells. The apoptosis rate in the ISO group was significantly increased, whereas HRM treatment inhibited cell apoptosis. However, tunicamycin reversed the antiapoptotic effect of HRM. Scale bar: 50 μm. (B) Percentage of TUNEL-positive cells. (C) Immunoblots for Bax and Bcl-2 proteins. (D, E) Quantified levels of Bax (D) and Bcl-2 (E) proteins. (F) Immunoblots showing the protein levels of GRP78, ATF4, and CHOP. (G–I) Quantification of GRP78 (G), ATF4 (H), and CHOP (I) protein expression. The data are expressed as the mean ± SEM (n = 3). *P < 0.05, **P < 0.01, vs. the control group; #P < 0.05, ##P < 0.01, vs. the ISO group; $^{@}P$ < 0.05, $^{@@}P$ < 0.01, vs. the ISO + 150 μM HRM + tunicamycin group (one-way analysis of variance followed by Tukey's $post\ hoc$ test). ATF4: Activating transcription factor 4; Bax: Bcl-2 associated X protein; Bcl-2: B-cell lymphoma-2; CHOP: C/EBP-homologous protein; DAPI: 4′,6-diamidino-2-phenylindole; GAPDH: glyceraldehyde-3-phosphate dehydrogenase; GRP78: glucose-related protein 78; HRM: hydrogen-rich culture medium; ISO: isoproterenol; Mg: magnesium; $MgCl_2$: magnesium chloride; Tm: tunicamycin; TUNEL: terminal dUTP nick end labeling.

ERS plays a critical role in the progression of HF,[74] as the accumulation of misfolded proteins in the ER triggers ERS and subsequent apoptosis.[75] GRP78, a molecular chaperone, typically binds to transmembrane proteins such as ATF6, IRE1, and PERK, keeping them inactive under normal conditions.[76] During ERS, GRP78 dissociates from ATF6, allowing it to be transported to the Golgi apparatus, where it is activated by S1P and S2P proteases.[77] This activation of ATF6 promotes the transcription of genes related to the unfolded protein response, including GRP78. Moreover, IRE1 is activated through phosphodimerization, and its endonuclease activity triggers mRNA splicing to produce X-box binding protein 1.[78] X-box binding protein 1 activates genes involved in ER protein folding, improving ER function.[79,80]

Additionally, GRP78 dissociation activates PERK, leading to the phosphorylation of eif2α, which subsequently activates ATF4, a transcriptional regulator involved in the upregulation of degradation genes.[81] ATF4, in turn, promotes the expression of CHOP,[82] a critical proapoptotic factor that downregulates antiapoptotic Bcl-2 while upregulating proapoptotic Bax.[83,84] This imbalance increases mitochondrial membrane permeability, leading to cytochrome C release and apoptosis.[85] CHOP further promotes apoptosis by inducing the expression of DNA damage-inducible protein 34, which contributes to protein misfolding and the generation of reactive oxygen species.[86]

The ERS-mediated apoptosis pathway is also related to the c-Jun N-terminal (JNK) and caspase pathways.[87] Upon activation, IRE1 forms a complex with TRAF2, which in turn activates the JNK cascade. This cascade regulates the apoptotic signaling regulating kinase 1, leading to the downregulation of Bcl-2 and the upregulation of Bax, further promoting apoptosis.[88,89] Under normal conditions, caspase-12 resides in the ER membrane as an inactive zymogen. Stress activates caspase-12, which translocates to the cytoplasm and activates caspase-3 through the cleavage of caspase-9, leading to apoptosis.[90] Moreover, CHOP can directly regulate the transcription of death receptor 5, a member of the TNF receptor family, triggering caspase-8-induced apoptosis.[85] Li et al.[91]showed that HRW can improve organ injury by inhibiting multiple signaling pathways related to ERS. This complex network of ERS-mediated pathways underscores potential therapeutic targets for interventions aimed at mitigating apoptosis in HFs.

Next, *in vitro*, we focused on ERS and apoptosis and found that ISO treatment increased the expression of GRP78, ATF4, and CHOP in H9C2 cardiomyocytes. HRM treatment, however, significantly reduced these levels, decreased Bax levels, and increased Bcl-2 expression, thereby inhibiting cardiomyocyte apoptosis. These findings were consistent across in *in vivo* models, as TUNEL staining confirmed that magnesium and HRW alleviated ISO-induced apoptosis in cardiomyocytes.

Tunicamycin, a nucleoside antibiotic, interferes with protein N-linked glycosylation, leading to the accumulation of misfolded proteins in the ER and subsequently triggering ERS.[92] To investigate the potential antiapoptotic effect of hydrogen through the inhibition of ERS, we introduced the ERS inducer tunicamycin to determine whether the protective effect of HRM on ISO-induced ERS in cells is related to its inhibition of ERS. Previous studies, including research by Liu et al.[93] have demonstrated that tunicamycin activates ERS, which is associated with nonalcoholic fatty liver disease. In our study, the introduction of tunicamycin negated the protective effects of HRM on H9C2 cardiomyocytes, as evidenced by decreases in cell viability and proliferation. Additionally, tunicamycin treatment resulted in the upregulation of ERS markers and promoted cell apoptosis. These results indicate that hydrogen plays a significant role in mitigating ERS, thereby providing antiapoptotic benefits to cardiomyocytes. Combined with the result of hydrogen release by magnesium, we propose that magnesium may protect against HF in rats through hydrogen, which exerts protective effects against ERS and apoptosis.

In conclusion, combined with the result of hydrogen release by magnesium, we propose that magnesium enhances heart function by releasing hydrogen, which mitigates ERS and apoptosis, offering new insights into HF treatment (**Figure 8**). This protective effect appears to be linked to the GRP78/ATF4/CHOP pathway. However, we cannot rule out the potential involvement of other pathways, such as the ATF6, IRE1, JNK, and caspase pathways, in mediating these effects. These findings indicate that magnesium could have therapeutic potential in both the prevention and treatment of HF. Furthermore, our study suggests that magnesium and magnesium-containing formulations may be viable candidates for drug development in this area. Our results may lay the foundation for further clinical exploration of the role of magnesium in HF, which is supported by animal-based research. However, additional studies are needed to fully evaluate the effectiveness and safety of magnesium across various animal models and clinical trials. We also recognize certain limitations in our study. We did not conduct hemodynamic monitoring, nor did we investigate the combined effect of hydrogen and Mg^{2+}. Further research is needed to explore additional mechanisms by which hydrogen may exert cardioprotective effects on HF. Additionally, we acknowledge that several factors could introduce biases and confounding variables into our research process. These factors include differences in animal weight, variations in the cage environment, the period of the experiment, and sample size. To improve the accuracy and reliability of future studies, we recommend using animals of similar weight, standardizing cage conditions, conducting experiments within a defined and consistent timeframe, and ensuring an adequate sample size whenever possible.

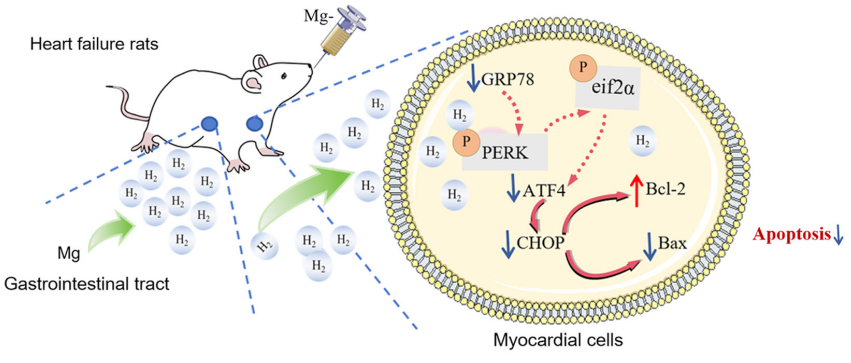

Figure 8 | The mechanism by which magnesium releases hydrogen to ameliorate heart failure.
ATF4: Activating transcription factor4; Bax: Bcl-2 associated X protein; Bcl-2: B-cell lymphoma-2; CHOP: C/EBP-homologous protein; eif2α: eukaryotic translation initiation factor 2α; GRP78: glucose-related protein78; Mg: magnesium; PERK: protein kinase RNA-like endoplasmic reticulum kinase.

Author contributions: *XZ, RT, FC, and RC designed the study, with FC and RC conducting the majority of the experiments and drafting the original draft. LY, BS, YW, YG, and RT contributed to additional experimental work. XZ and RT reviewed and edited the manuscript. All authors read and approved the final manuscript.*

Conflicts of interest: *The authors declare no conflict of interest.*

Data availability statement: *All data generated or analyzed during this study are included in this paper.*

References

1. Savarese G, Becher PM, Lund LH, Seferovic P, Rosano GMC, Coats AJS. Global burden of heart failure: a comprehensive and updated review of epidemiology. *Cardiovasc Res.* 2023;118:3272-3287.
2. Jiang H, Fang T, Cheng Z. Mechanism of heart failure after myocardial infarction. *J Int Med Res.* 2023;51:3000605231202573.
3. Cai Q, Li Y, Zhang Y, et al. Xinshubao tablet ameliorates myocardial injury against heart failure via the DCN/PPARα/PGC-1α/P300 pathway. *Biomed Pharmacother.* 2023;166:115285.
4. Wang Q, Liang S, Qian J, et al. OTUD1 promotes isoprenaline- and myocardial infarction-induced heart failure by targeting PDE5A in cardiomyocytes. *Biochim Biophys Acta Mol Basis Dis.* 2024;1870:167018.
5. Chouairi F, Levin A, Biegus J, Fudim M. Emerging devices for heart failure management. *Prog Cardiovasc Dis.* 2024;82:125-134.
6. Stretti L, Zippo D, Coats AJS, et al. A year in heart failure: an update of recent findings. *ESC Heart Fail.* 2021;8:4370-4393.
7. McDonagh TA, Metra M, Adamo M, et al. 2021 ESC Guidelines for the diagnosis and treatment of acute and chronic heart failure. *Eur Heart J.* 2021;42:3599-3726.
8. Fan M, Zhang J, Zeng L, et al. Non-coding RNA mediates endoplasmic reticulum stress-induced apoptosis in heart disease. *Heliyon.* 2023;9:e16246.
9. Momot K, Krauz K, Czarzasta K, et al. Post-myocardial infarction heart failure and long-term high-fat diet: Cardiac endoplasmic reticulum stress and unfolded protein response in Sprague Dawley rat model. *PLoS One.* 2024;19:e0308833.
10. Zheng H, Yin Z, Luo X, Zhou Y, Zhang F, Guo Z. Associations between systemic immunity-inflammation index and heart failure: Evidence from the NHANES 1999-2018. *Int J Cardiol.* 2024;395:131400.
11. Chen J, Wei X, Zhang Q, et al. The traditional Chinese medicines treat chronic heart failure and their main bioactive constituents and mechanisms. *Acta Pharm Sin B.* 2023;13:1919-1955.
12. Zhang SX, Wang JJ, Starr CR, et al. The endoplasmic reticulum: Homeostasis and crosstalk in retinal health and disease. *Prog Retin Eye Res.* 2024;98:101231.
13. Wang S, Binder P, Fang Q, et al. Endoplasmic reticulum stress in the heart: insights into mechanisms and drug targets. *Br J Pharmacol.* 2018;175:1293-1304.
14. Ren J, Bi Y, Sowers JR, Hetz C, Zhang Y. Endoplasmic reticulum stress and unfolded protein response in cardiovascular diseases. *Nat Rev Cardiol.* 2021;18:499-521.
15. Stitziel NO, Kanter JE, Bornfeldt KE. Emerging targets for cardiovascular disease prevention in diabetes. *Trends Mol Med.* 2020;26:744-757.
16. Wang S, Xu F, Liu H, et al. Suppressing endoplasmic reticulum stress alleviates LPS-induced acute lung injury via inhibiting inflammation and ferroptosis. *Inflammation.* 2024;47:1067-1082.
17. Qi M, Jiang Q, Yang S, et al. The endoplasmic reticulum stress-mediated unfolded protein response protects against infection of goat endometrial epithelial cells by Trueperella pyogenes via autophagy. *Virulence.* 2022;13:122-136.
18. Tang Q, Liu Q, Li Y, Mo L, He J. CRELD2, endoplasmic reticulum stress, and human diseases. *Front Endocrinol (Lausanne).* 2023;14:1117414.
19. Xu J, Zhao L, Zhang X, et al. Salidroside ameliorates acetaminophen-induced acute liver injury through the inhibition of endoplasmic reticulum stress-mediated ferroptosis by activating the AMPK/SIRT1 pathway. *Ecotoxicol Environ Saf.* 2023;262:115331.
20. Whelan RS, Kaplinskiy V, Kitsis RN. Cell death in the pathogenesis of heart disease: mechanisms and significance. *Annu Rev Physiol.* 2010;72:19-44.
21. Chen J, Liu Y, Pan D, et al. Estrogen inhibits endoplasmic reticulum stress and ameliorates myocardial ischemia/reperfusion injury in rats by upregulating SERCA2a. *Cell Commun Signal.* 2022;20:38.
22. Wu S, Lu D, Gajendran B, et al. Tanshinone IIA ameliorates experimental diabetic cardiomyopathy by inhibiting endoplasmic reticulum stress in cardiomyocytes via SIRT1. *Phytother Res.* 2023;37:3543-3558.
23. Monceaux K, Gressette M, Karoui A, et al. Ferulic acid, pterostilbene, and tyrosol protect the heart from ER-stress-induced injury by activating SIRT1-dependent deacetylation of eIF2α. *Int J Mol Sci.* 2022;23:6628.
24. Yuan T, Zhao JN, Bao NR. Hydrogen applications: advances in the field of medical therapy. *Med Gas Res.* 2023;13:99-107.
25. Yu Y, Feng J, Lian N, et al. Hydrogen gas alleviates blood-brain barrier impairment and cognitive dysfunction of septic mice in an Nrf2-dependent pathway. *Int Immunopharmacol.* 2020;85:106585.
26. Ohsawa I, Ishikawa M, Takahashi K, et al. Hydrogen acts as a therapeutic antioxidant by selectively reducing cytotoxic oxygen radicals. *Nat Med.* 2007;13:688-694.
27. Johnsen HM, Hiorth M, Klaveness J. Molecular hydrogen therapy-a review on clinical studies and outcomes. *Molecules.* 2023;28:7785.
28. Wu C, Zou P, Feng S, et al. Molecular hydrogen: an emerging therapeutic medical gas for brain disorders. *Mol Neurobiol.* 2023;60:1749-1765.
29. Cheng J, Shi M, Sun X, Lu H. Therapeutic effect of hydrogen and its mechanisms in kidney disease treatment. *Med Gas Res.* 2024;14:48-53.
30. Chen Y, Wei Y, Tang W. The role of hydrogen in the prevention and treatment of coronary atherosclerotic heart disease. *Eur J Pharmacol.* 2024;972:176586.
31. Takefuji Y. Hydrogen inhalation therapy for inflammation and eye diseases: a review of the literature. *Eye (Lond).* 2024;38:2497-2498.
32. Fu Z, Zhang J, Zhang Y. Role of molecular hydrogen in ageing and ageing-related diseases. *Oxid Med Cell Longev.* 2022;2022:2249749.
33. Lu Z, Lin Y, Peng B, Bao Z, Niu K, Gong J. Hydrogen-rich saline ameliorates hepatic ischemia-reperfusion injury through regulation of endoplasmic reticulum stress and apoptosis. *Dig Dis Sci.* 2017;62:3479-3486.
34. Dhillon G, Buddhavarapu V, Grewal H, et al. Hydrogen water: extra healthy or a hoax?-A systematic review. *Int J Mol Sci.* 2024;25:973.
35. Jiang S, Fan Q, Xu M, et al. Hydrogen-rich saline protects intestinal epithelial tight junction barrier in rats with intestinal ischemia-reperfusion injury by inhibiting endoplasmic reticulum stress-induced apoptosis pathway. *J Pediatr Surg.* 2020;55:2811-2819.
36. Li C, Cao Y, Kohei F, et al. Nano-bubble hydrogen water: an effective therapeutic agent against inflammation related disease caused by viral infection in zebrafish model. *Virol Sin.* 2022;37:277-283.
37. Htun Y, Nakamura S, Nakao Y, et al. Hydrogen ventilation combined with mild hypothermia improves short-term neurological outcomes in a 5-day neonatal hypoxia-ischaemia piglet model. *Sci Rep.* 2019;9:4088.
38. Guo JD, Li L, Shi YM, Wang HD, Hou SX. Hydrogen water consumption prevents osteopenia in ovariectomized rats. *Br J Pharmacol.* 2013;168:1412-1420.
39. Xu C, Wang S, Wang H, et al. Magnesium-based micromotors as hydrogen generators for precise rheumatoid arthritis therapy. *Nano Lett.* 2021;21:1982-1991.
40. Wang JL, Xu JK, Hopkins C, Chow DH, Qin L. Biodegradable magnesium-based implants in orthopedics-a general review and perspectives. *Adv Sci (Weinh).* 2020;7:1902443.
41. Zhou H, He Z, Cao Y, et al. An injectable magnesium-loaded hydrogel releases hydrogen to promote osteoporotic bone repair via ROS scavenging and immunomodulation. *Theranostics.* 2024;14:3739-3759.
42. Yu Y, Wang WN, Han HZ, Xie KL, Wang GL, Yu YH. Protective effects of hydrogen-rich medium on lipopolysaccharide-induced monocytic adhesion and vascular endothelial permeability through regulation of vascular endothelial cadherin. *Genet Mol Res.* 2015;14:6202-6212.
43. Yang T, Wang L, Sun R, et al. HYdrogen-rich medium ameliorates lipopolysaccharide-induced barrier dysfunction via rhoa-Mdia1 signaling in Caco-2 cells. *Shock.* 2016;45:228-237.
44. Percie du Sert N, Hurst V, Ahluwalia A, et al. The ARRIVE guidelines 2.0: Updated guidelines for reporting animal research. *PLoS Biol.* 2020;18:e3000410.
45. Yao X, Chen D, Zhao B, et al. Acid-degradable hydrogen-generating metal-organic framework for overcoming cancer resistance/metastasis and off-target side effects. *Adv Sci (Weinh).* 2022;9:e2101965.

46. Meng X, Liu Z, Deng L, et al. Hydrogen therapy reverses cancer-associated fibroblasts phenotypes and remodels stromal microenvironment to stimulate systematic anti-tumor immunity. *Adv Sci (Weinh).* 2024;11:e2401269.
47. Chen S, Zhu Y, Xu Q, et al. Photocatalytic glucose depletion and hydrogen generation for diabetic wound healing. *Nat Commun.* 2022;13:5684.
48. He Y, Zhang B, Chen Y, et al. Image-guided hydrogen gas delivery for protection from myocardial ischemia-reperfusion injury via microbubbles. *ACS Appl Mater Interfaces.* 2017;9:21190-21199.
49. Hayashida K, Sano M, Ohsawa I, et al. Inhalation of hydrogen gas reduces infarct size in the rat model of myocardial ischemia-reperfusion injury. *Biochem Biophys Res Commun.* 2008;373:30-35.
50. Schneider CA, Rasband WS, Eliceiri KW. NIH Image to ImageJ: 25 years of image analysis. *Nat Methods.* 2012;9:671-675.
51. Aoyagi T, Matsui T. Phosphoinositide-3 kinase signaling in cardiac hypertrophy and heart failure. *Curr Pharm Des.* 2011;17:1818-1824.
52. Spitz AZ, Gavathiotis E. Physiological and pharmacological modulation of BAX. *Trends Pharmacol Sci.* 2022;43:206-220.
53. Szymanski MW, Singh DP. Isoproterenol. *StatPearls*. Treasure Island (FL): StatPearls Publishing; 2025.
54. Tan R, You Q, Cui J, et al. Sodium houttuyfonate against cardiac fibrosis attenuates isoproterenol-induced heart failure by binding to MMP2 and p38. *Phytomedicine.* 2023;109:154590.
55. Abdelrahaman D, Habotta OA, Taher ES, et al. Suppression of NLRP3 inflammasome orchestrates the protective efficacy of tiron against isoprenaline-induced myocardial injury. *Front Pharmacol.* 2024;15:1379908.
56. Gao W, Guo N, Yan H, Zhao S, Sun Y, Chen Z. Mycn ameliorates cardiac hypertrophy-induced heart failure in mice by mediating the USP2/JUP/Akt/β-catenin cascade. *BMC Cardiovasc Disord.* 2024;24:82.
57. Qian K, Tang J, Ling YJ, et al. Exogenous NADPH exerts a positive inotropic effect and enhances energy metabolism via SIRT3 in pathological cardiac hypertrophy and heart failure. *EBioMedicine.* 2023;98:104863.
58. Li L, Ye J, Zhao Z, et al. Shenfu injection improves isoproterenol-induced heart failure in rats by modulating co-metabolism and regulating the trimethylamine-N-oxide - inflammation axis. *Front Pharmacol.* 2024;15:1412300.
59. Pouleur AC, Menghoum N, Cumps J, et al. Plasma myo-inositol elevation in heart failure: clinical implications and prognostic significance. Results from the BElgian and CAnadian MEtabolomics in HFpEF (BECAME-HF) research project. *EBioMedicine.* 2024;107:105264.
60. Crnko S, Printezi MI, Zwetsloot PM, et al. The circadian clock remains intact, but with dampened hormonal output in heart failure. *EBioMedicine.* 2023;91:104556.
61. Kresoja KP, Unterhuber M, Wachter R, et al. Treatment response to spironolactone in patients with heart failure with preserved ejection fraction: a machine learning-based analysis of two randomized controlled trials. *EBioMedicine.* 2023;96:104795.
62. Bayes-Genis A, Docherty KF, Petrie MC, et al. Practical algorithms for early diagnosis of heart failure and heart stress using NT-proBNP: A clinical consensus statement from the Heart Failure Association of the ESC. *Eur J Heart Fail.* 2023;25:1891-1898.
63. Castiglione V, Aimo A, Vergaro G, Saccaro L, Passino C, Emdin M. Biomarkers for the diagnosis and management of heart failure. *Heart Fail Rev.* 2022;27:625-643.
64. Núñez J, de la Espriella R, Rossignol P, et al. Congestion in heart failure: a circulating biomarker-based perspective. A review from the Biomarkers Working Group of the Heart Failure Association, European Society of Cardiology. *Eur J Heart Fail.* 2022;24:1751-1766.
65. Pan L, Xu Z, Wen M, et al. Xinbao Pill ameliorates heart failure via regulating the SGLT1/AMPK/PPARα axis to improve myocardial fatty acid energy metabolism. *Chin Med.* 2024;19:82.
66. Liao M, Xie Q, Zhao Y, et al. Main active components of Si-Miao-Yong-An decoction (SMYAD) attenuate autophagy and apoptosis via the PDE5A-AKT and TLR4-NOX4 pathways in isoproterenol (ISO)-induced heart failure models. *Pharmacol Res.* 2022;176:106077.
67. Li J, Angsantikul P, Liu W, et al. Micromotors spontaneously neutralize gastric acid for pH-responsive payload release. *Angew Chem Int Ed Engl.* 2017;56:2156-2161.
68. Negru AG, Pastorcici A, Crisan S, Cismaru G, Popescu FG, Luca CT. The role of hypomagnesemia in cardiac arrhythmias: a clinical perspective. *Biomedicines.* 2022;10:2356.
69. Yu W, Ding J, Chen J, et al. Magnesium ion-doped mesoporous bioactive glasses loaded with gallic acid against myocardial ischemia/reperfusion injury by affecting the biological functions of multiple cells. *Int J Nanomedicine.* 2024;19:347-366.
70. Aboalgasm H, Petersen M, Gwanyanya A. Improvement of cardiac ventricular function by magnesium treatment in chronic streptozotocin-induced diabetic rat heart. *Cardiovasc J Afr.* 2021;32:141-148.
71. Martens P, Ferreira JP, Vincent J, et al. Prognostic relevance of magnesium alterations in patients with a myocardial infarction and left ventricular dysfunction: insights from the EPHESUS trial. *Eur Heart J Acute Cardiovasc Care.* 2022;11:148-159.
72. Magnesium in Coronaries (MAGIC) Trial Investigators. Early administration of intravenous magnesium to high-risk patients with acute myocardial infarction in the Magnesium in Coronaries (MAGIC) Trial: a randomised controlled trial. *Lancet.* 2002;360:1189-1196.
73. Song R, Xiong C, Bai J, Bai Z, Liu W. Artemisinin attenuates isoproterenol-induced cardiac hypertrophy via the ERK1/2 and p38 MAPK signaling pathways. *Curr Mol Pharmacol.* 2023. doi: 10.2174/0118761429244886230927070818.
74. Hu L, Gao D, Lv H, et al. Finding new targets for the treatment of heart failure: endoplasmic reticulum stress and autophagy. *J Cardiovasc Transl Res.* 2023;16:1349-1356.
75. Chen Z, Zhang SL. Endoplasmic reticulum stress: a key regulator of cardiovascular disease. *DNA Cell Biol.* 2023;42:322-335.
76. Tian Q, Liu J, Chen Q, Zhang M. Andrographolide contributes to the attenuation of cardiac hypertrophy by suppressing endoplasmic reticulum stress. *Pharm Biol.* 2023;61:61-68.
77. Ye J, Rawson RB, Komuro R, et al. ER stress induces cleavage of membrane-bound ATF6 by the same proteases that process SREBPs. *Mol Cell.* 2000;6:1355-1364.
78. Calfon M, Zeng H, Urano F, et al. IRE1 couples endoplasmic reticulum load to secretory capacity by processing the XBP-1 mRNA. *Nature.* 2002;415:92-96.
79. Yamamoto K, Sato T, Matsui T, et al. Transcriptional induction of mammalian ER quality control proteins is mediated by single or combined action of ATF6alpha and XBP1. *Dev Cell.* 2007;13:365-376.
80. Iurlaro R, Muñoz-Pinedo C. Cell death induced by endoplasmic reticulum stress. *FEBS J.* 2016;283:2640-2652.
81. Tang H, Kang R, Liu J, Tang D. ATF4 in cellular stress, ferroptosis, and cancer. *Arch Toxicol.* 2024;98:1025-1041.
82. Xu D, Liu Z, Liang MX, et al. Endoplasmic reticulum stress targeted therapy for breast cancer. *Cell Commun Signal.* 2022;20:174.
83. Ajoolabady A, Kaplowitz N, Lebeaupin C, et al. Endoplasmic reticulum stress in liver diseases. *Hepatology.* 2023;77:619-639.
84. Ma N, Lu H, Li N, et al. CHOP-mediated Gasdermin E expression promotes pyroptosis, inflammation, and mitochondrial damage in renal ischemia-reperfusion injury. *Cell Death Dis.* 2024;15:163.
85. Yang Y, Liu L, Naik I, Braunstein Z, Zhong J, Ren B. Transcription factor C/EBP homologous protein in health and diseases. *Front Immunol.* 2017;8:1612.
86. Li J, Inoue R, Togashi Y, et al. Imeglimin ameliorates β-cell apoptosis by modulating the endoplasmic reticulum homeostasis pathway. *Diabetes.* 2022;71:424-439.
87. Ding W, Zhang X, Huang H, et al. Adiponectin protects rat myocardium against chronic intermittent hypoxia-induced injury via inhibition of endoplasmic reticulum stress. *PLoS One.* 2014;9:e94545.
88. Yoshida H, Matsui T, Yamamoto A, Okada T, Mori K. XBP1 mRNA is induced by ATF6 and spliced by IRE1 in response to ER stress to produce a highly active transcription factor. *Cell.* 2001;107:881-891.
89. Lee AH, Iwakoshi NN, Glimcher LH. XBP-1 regulates a subset of endoplasmic reticulum resident chaperone genes in the unfolded protein response. *Mol Cell Biol.* 2003;23:7448-7459.
90. Liu MQ, Chen Z, Chen LX. Endoplasmic reticulum stress: a novel mechanism and therapeutic target for cardiovascular diseases. *Acta Pharmacol Sin.* 2016;37:425-443.
91. Li H, Bai G, Ge Y, et al. Hydrogen-rich saline protects against small-scale liver ischemia-reperfusion injury by inhibiting endoplasmic reticulum stress. *Life Sci.* 2018;194:7-14.
92. Banerjee DK, Seijo Lebrón A, Baksi K. Glycotherapy: a new paradigm in breast cancer research. *Biomolecules.* 2022;12:487.
93. Liu C, Zhou B, Meng M, et al. FOXA3 induction under endoplasmic reticulum stress contributes to non-alcoholic fatty liver disease. *J Hepatol.* 2021;75:150-162.